

A Three-Dimensional Cellular Automaton–Finite Element Model for the Prediction of Solidification Grain Structures

Ch.-A. GANDIN, J.-L. DESBIOLLES, M. RAPPAZ, and Ph. THEVOZ

A three-dimensional (3-D) model for the prediction of dendritic grain structures formed during solidification is presented. This model is built on the basis of a 3-D cellular automaton (CA) algorithm. The simulation domain is subdivided into a regular lattice of cubic cells. Using physically based rules for the simulation of nucleation and growth phenomena, a state index associated with each cell is switched from zero (liquid state) to a positive value (mushy and solid state) as solidification proceeds. Because these physical phenomena are related to the temperature field, the cell grid is superimposed to a coarser finite element (FE) mesh used for the solution of the heat flow equation. Two coupling modes between the microscopic CA and macroscopic FE calculations have been designed. In a so-called “weak” coupling mode, the temperature of each cell is simply interpolated from the temperature of the FE nodes using a unique solidification path at the macroscopic scale. In a “full” coupling mode, the enthalpy field is also interpolated from the FE nodes to the CA cells and a fraction of solid increment is computed for each mushy cell using a truncated Scheil microsegregation model. These fractions of solid increments are then fed back to the FE nodes in order to update the new temperature field, thus accounting for a more realistic release of the latent heat (*i.e.*, the solidification path is no longer unique). Special dynamic allocation techniques have been designed in order to minimize the computation costs and memory size associated with a very large number of cells (typically 10^7 to 10^8). The potentiality of the CAFE model is demonstrated through the predictions of typical grain structures formed during the investment casting and continuous casting processes.

I. INTRODUCTION

A two-dimensional (2-D) cellular automaton (CA)–finite element (FE) model has been proposed by Gandin and Rappaz for the modeling of dendritic grain structures formation during solidification.^[1] This 2-D CAFE model was validated on the basis of numerical tests performed on simple heat flow configurations, *e.g.*, Bridgman-type cooling conditions (fixed thermal gradient and cooling rate). These tests were complemented by the comparison of the predicted envelopes of single dendritic grains with those calculated from analytical solutions.^[2] Experimental validations were also carried out using *in situ* observations of the Bridgman solidification of transparent analogues. The 2-D CA algorithm was shown to reproduce well the growth competition occurring among columnar grains.^[1] Good agreement was also obtained for the extension of a single dendritic grain into a lateral region of liquid past a re-entrant corner.^[2] The predicted columnar-to-equiaxed transition using the 2-D CAFE model was finally compared with the grain structure of an aluminum - 7 wt pct silicon alloy, which was unidirectionally solidified. As a result of these various validations, it was concluded that (1) the 2-D CA growth algorithm is indeed able to account for the physical mechanisms involved during dendritic growth (*e.g.*, influence of the dendrite growth direction on the tip

undercooling, grain competition at grain boundary, *etc.*); and (2) the 2-D CAFE model can predict satisfactorily the grain structures formed in various solidification processes such as the investment casting of turbine blades, the continuous casting of rods, and welding.^[3]

Despite the new insight brought by the 2-D CAFE model into the modeling of solidification grain structures, a three-dimensional (3-D) model had yet to be developed in order to predict quantitatively real as-cast structures. Indeed, the 2-D model could reproduce neither the intricacy of grain structures seen in transverse sections of thin “equiaxed” plates or airfoils nor the evolution of the crystallographic texture associated with the selection mechanisms of columnar grains. This problem was partially overcome by considering a preliminary 3-D extension of the CA model, yet limited to uniform temperature situations and simple geometry.^[4,5,6] But a general extension of the CAFE model to 3-D heat flow situations in real casting geometry had still to be made.

A major step in this direction was achieved recently by Gandin and Rappaz, who proposed a 3-D CA growth algorithm of dendritic grains valid for any arbitrary temperature field.^[7] As for the 2-D developments, it was shown that the predictions of the new 3-D CA growth model compared favorably with an analytical solution developed under the assumption of Bridgman-type cooling conditions. In their conclusion, Gandin and Rappaz wrote: “the 3D CA growth algorithm, coupled with Finite Element heat flow calculations, will become a major tool for the prediction of dendritic grain structures in solidification processes.” However, the coupling of a 3-D CA nucleation-growth model with a FE heat flow model is not straightforward due to the very large number of cells involved in a casting. Indeed, it was shown in 2-D that the typical cell size that is required to reproduce well the branching mechanisms of dendrite arms (and thus

Ch.-A. GANDIN, formerly with the Laboratoire de Metallurgie Physique, Departement des Materiaux, Ecole Polytechnique Federale de Lausanne, Switzerland, is with the Ecole des Mines, Parc de Saurupt, F-54042 Nancy, France. J.-L. DESBIOLLES, Staff Member, and M. RAPPAZ, Professor, are with the Laboratoire de Metallurgie Physique, Departement des Materiaux, Ecole Polytechnique Federale de Lausanne, CH-1015 Lausanne, Switzerland. Ph. THEVOZ, Executive Director, is with Calcom SA, PSE-EPFL, CH-1015 Lausanne, Switzerland.

Manuscript submitted April 14, 1999.

grain competition) is of the order of 50 to 100 μm . For a 3-D casting of only $(10 \times 10 \times 10) \text{ cm}^3$, this means that 1 to 8 billions cubic cells would have to be defined with typically 100 bytes of information per cell. In order to overcome such difficulties, specific numerical techniques had to be implemented in a 3-D CAFE model. The goal of this article is to present the special coupling that has been achieved between the 3-D CA model and FE heat flow simulation and to demonstrate its feasibility for the investment casting and continuous casting processes.

II. A 3-D CA MODEL

As for 2-D geometry, the 3-D CA model first requires subdivision of the simulation domain, in which solidification takes place into a regular lattice of cubic cells. A state index, I_ν , is attributed to each cell, ν . At the beginning of the calculation, the metal is liquid and all the cells have a zero state index. By defining appropriate rules to change the value of the state index of the cells, a phase transformation can be simulated.^[8] As in the Monte Carlo method,^[9–12] these rules can be based on probabilities, which might be a function of the temperature and state of the nearest neighbors (NNs), or they can be deterministic as in the CA method. In any case, they should reflect the physical phenomena involved in the solidification of dendritic alloys and summarized in classical textbooks.^[13] The only stochastic aspects built in the present CA model, which can be verified experimentally,^[6] are related to nucleation because both the position and crystallographic orientation of a new nucleus are usually dependent on hidden variables (except, for example, in Bridgman directional solidification with a seed crystal or more generally in epitaxial growth). The nucleation and growth algorithms used in the 3-D CA, which are largely based on the 2-D model,^[1] are briefly presented hereafter.

A. Nucleation Algorithm

As for the previous 2-D CA model,^[1] the nucleation algorithm built into the 3-D CA model is based on an instantaneous nucleation model proposed by Rappaz.^[14] This model relies on two observations. First, at the small undercoolings usually encountered in castings, the heterogeneous nucleation theory proposed by Turnbull^[15] predicts an abrupt burst of nucleation as soon as a critical undercooling is reached. It can be approximated consequently by an instantaneous activation of the corresponding nucleation sites at this undercooling. Second, several families of nucleation sites, all characterized by different critical undercoolings, usually coexist in the melt. However, it seems difficult, if not impossible, to make an “inventory” of all these families. Consequently, Rappaz proposed to consider a Gaussian distribution of nucleation sites to model the grain density increase, dn , which is induced by an increase in the undercooling, $d(\Delta T)$.^[14] The distribution, $dn/d(\Delta T)$, is described by its mean undercooling, ΔT_N , its standard deviation, ΔT_σ , and its integral, n_{max} . This latter value corresponds to the maximum grain density, which can be reached if all the nucleation site families are activated during the cooling process. These parameters have to be determined experimentally for a given alloy.^[14]

In an initialization stage, nucleation sites are distributed

among the cells defining the CA grid. For that purpose, the number of nucleation sites, N_V^{nuc} , to be distributed among the cells of a given volume V is simply given by $(n_{\text{max}}V)$, these cells being randomly chosen in the volume V . For each “nucleation cell” ν selected in this way, a nucleation undercooling, $\Delta T_\nu^{\text{nuc}} = T_L - T_\nu^{\text{nuc}}$, where T_L is the liquidus temperature and T_ν^{nuc} is the critical nucleation temperature, is also randomly attributed according to the prescribed Gaussian distribution, $dn/d(\Delta T)$. Unlike the 2-D CAFE model for which all the cells are defined at the beginning of the calculation (*i.e.*, V in this case is the entire volume of the casting), the 3-D CAFE algorithm uses a dynamic allocation of the cells (Section IV). Therefore, initialization of nucleation cells is repeated every time new liquid cells (and thus liquid volume) are dynamically allocated during the CA calculation.

If no nucleation site is located in a cell, no nucleation event can take place in it regardless of its temperature. On the contrary, if the temperature of a nucleation cell ν , T_ν , becomes lower than the critical temperature of its “associated” nucleation site, T_ν^{nuc} , the value of the state index of the cell, I_ν , is changed to a nonzero integer value identical to the grain counter index. A crystallographic orientation is then randomly chosen among predefined orientation classes. These orientation classes are initialized at the beginning of the calculation by a random selection of the three Euler angles (refer to the definition in Reference 16) producing a uniform distribution of the $\langle 100 \rangle$ directions on a unit sphere.

It should be mentioned that during the random selection of N_V^{nuc} cells, some cells may be selected twice or more. In such a case, only the smaller nucleation undercooling, *i.e.*, the most favorable nucleation site, is kept in agreement with the instantaneous nucleation law. Nucleation at boundaries of the casting can also be defined in a similar way by using as many Gaussian distributions as necessary, the cells located at a boundary being identified by an additional boundary index, I_{Ref} , equal to the reference of the boundary to which they belong ($I_{\text{Ref}} = 0$ if the cell is in the bulk of the liquid). The maximum volume grain density is then replaced by a maximum surface grain density and the number of nucleation sites to be distributed, N_S^{nuc} , is calculated by considering the surface of the domain, S , on which the reference applies.

Other nucleation boundary conditions can be described in the 3-D CAFE model, as summarized in Table I. “Single crystal” boundary conditions allow the start of formation of the “grain structure” (*i.e.*, of only one grain if no stray crystal forms) for a specified undercooling and crystallographic orientation, either on a referenced surface or at a specified location in the casting. This is of practical use when only the growth of a single crystal is to be studied (*e.g.*, propagation of a single crystal in the platform of an investment cast turbine blade). The “ $\langle 100 \rangle$ fiber texture” boundary condition applies only for a surface; in this case, the crystallographic orientation classes of the grains for this surface are generated by assuming an initial fiber texture (table footnote).

B. Growth Algorithm

As for the 2-D CAFE model, the 3-D CA growth algorithm must be able to reproduce the preferential $\langle 100 \rangle$ growth directions of fcc dendrites and their growth kinetics. It is based on the growth of an octahedron bounded by (111) faces and is applied to each cell having a nonzero state index

Table I. Nucleation Conditions Available in the 3-D CAFE Model and Associated Parameters*

Type	Location	Parameters
Gaussian distribution	volume	$(\Delta T_N, \Delta T_\sigma, n_{\max})$ Units: (K, K, m^{-3})
Gaussian distribution	surface	$I_{\text{Ref}}, (\Delta T_N, \Delta T_\sigma, n_{\max})$ Units: —, (K, K, m^{-2})
Single crystal	surface	$I_{\text{Ref}}, (\phi_1, \phi, \phi_2), \Delta T_n$ Units: —, (deg, deg, deg), K
Single crystal	point	$(\phi_1, \phi, \phi_2), \Delta T_n, (x, y, z)$ Units: (deg, deg, deg), K, (m, m, m)
$\langle 100 \rangle$ fiber texture	surface	$I_{\text{Ref}}, n_g, (n_x, n_y, n_z), \theta$ Units: —, m^{-2} , (m, m, m), deg

* $(\Delta T_N, \Delta T_\sigma, n_{\max})$ are the three parameters of a Gaussian distribution of nucleation sites as a function of the undercooling (mean value, standard deviation, and maximum grain density, respectively).^[14] I_{Ref} is a cell reference number; (ϕ_1, ϕ, ϕ_2) are the three Euler angles defining the crystallographic orientation of a single crystal; ΔT_n is the nucleation undercooling of a single crystal; n_g is a surface grain density; and (n_x, n_y, n_z) is the axis of a $\langle 100 \rangle$ fiber texture, *i.e.*, (n_x, n_y, n_z) are the direction cosines in the (X, Y, Z) reference of a direction around which the $[001]$ trunk directions of the grains are randomly distributed within a solid angle, θ ($\theta \leq 45$ deg). The $[100]$ directions (and consequently the $[010]$ directions) are randomly selected in the plane perpendicular to (n_x, n_y, n_z) .

and at least one neighboring liquid cell.^[7] This is shown schematically in Figure 1: the growing octahedron associated with a cell ν ($I_\nu \neq 0$) is “capturing” the cell center of one of its neighbors μ ($I_\mu = 0$). The state index of the cell μ is then switched to that of the parent cell ν (*i.e.*, $I_\mu = I_\nu$), and the growth of a new octahedron associated with cell μ is later considered. As soon as a cell is fully surrounded by

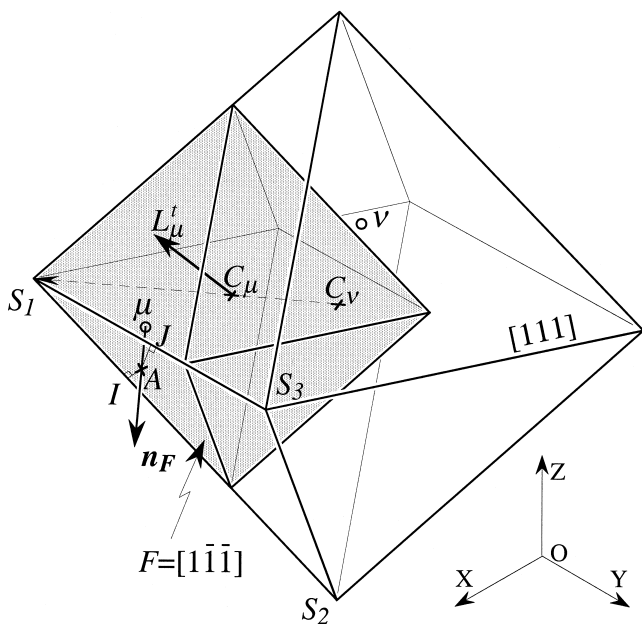


Fig. 1—Schematics of the decentered octahedron CA growth algorithm.^[7]

mushy cells, the growth of its associated octahedron is no longer considered.

The main diagonals of the octahedron correspond to the $\langle 100 \rangle$ crystallographic orientations along which dendrite stems and arms of fcc metals preferentially develop. Their extension is calculated by integrating over time the growth law of the dendrite tips given by the model of Kurz *et al.*^[17,18] Thus, within the time-step, δt , used for integrating the growth kinetics of the dendrite tips, the size increment of the diagonals of the octahedron associated with a cell ν , ΔR_ν , is given by

$$\Delta R_\nu = v(\Delta T_\nu) \delta t \quad [1]$$

where $v(\Delta T_\nu)$ is the velocity of the dendrite tips calculated for the corresponding undercooling, ΔT_ν , of cell ν . In the case of an octahedron whose diagonals are perfectly aligned with the (X, Y, Z) axes of the CA grid, the CA growth algorithm can be simply applied to the center of the cells. In a uniform temperature field, this integration leads to a simple octahedral shape in agreement with the experimental observations of Ovsienko *et al.*^[19] But the main problem associated with the design of a CA growth algorithm capable of keeping the preferential growth directions of the dendrites is highlighted when trying to propagate a grain with a randomly chosen crystallographic orientation with respect to the axes of the CA grid. The strong anisotropy introduced by the cubic cell lattice leads to a grain shape always aligned with the CA grid, the growth kinetics being no longer properly integrated over time. In order to correct the anisotropy introduced by the cubic cell lattice, Gandin and Rappaz have proposed the use of a decentered octahedron growth algorithm.^[7] This is schematically shown in Figure 1: the centers, C_ν and C_μ , of the growth octahedra associated with cells ν and μ do not coincide with their centers. Details of this algorithm can be found in Reference 7. It should be also noted that the growth kinetics, $v(\Delta T_\nu)$, of the six dendrite tips of a given octahedron are the same; they are evaluated using the temperature T_ν (or the undercooling ΔT_ν) of the center of cell ν . This approximation, however, is reasonable as shown by the validations reported in Reference 7. Finally, the growth algorithm is applied with an environment given by the 6 first-, 12 second-, and 8 third-NN cells (26 neighbor cells).

C. Micro Time-Step Calculation

In order to correctly integrate the growth kinetics and propagate the crystallographic orientation of the grain, the extension of the octahedron associated with a cell ν during one time-step must be restricted to the NN. If δt is the micro-time-step used for the integration of the growth kinetics, the criterion introduced by the CA growth algorithm can be written as

$$\delta t \leq \delta t_{\max} \quad [2]$$

where

$$\delta t_{\max} = l_{\text{cell}}/v(\Delta T_{\max}) \quad [3]$$

The maximum value of the time-step used for the integration of the growth kinetics, δt_{\max} , is thus given by the ratio of the cell size, l_{cell} , and the highest dendrite tip velocity, $v(\Delta T_{\max})$, taken at the maximum undercooling, ΔT_{\max} , of all the growth cells found in the simulation domain.

This criterion is valid when considering individual grains. However, two adjacent growth cells, ν_1 and ν_2 , belonging to two different grains (*i.e.*, cells located on both sides of a grain boundary), may both be able to capture a common liquid neighboring cell, μ , during the same time-step. Because all the growth cells are successively scanned within one micro-time-step, the first scanned cell would then capture cell μ , regardless of the crystallographic orientations of the grains. In order to overcome this problem and correctly predict the growth competition of columnar grains, a parameter, α , has been introduced in the selection of the micro-time-step, δt , used for the integration of the dendrite tips kinetics. One then has

$$\delta t = \alpha \delta t_{\max} \quad \text{with } \alpha \in]0, 1] \quad [4]$$

III. COUPLING CALCULATION MODES

As for the 2-D CAFE model,^[1] the heat exchanges are calculated at the level of a coarse FE mesh, whereas nucleation and growth are simulated at the fine CA grid level. Various coupling schemes have been implemented in the 3-D CAFE model.

A. Weak Coupling Calculation Mode: Temperature Interpolations

As shown previously, the nucleation and growth algorithms are defined as a function of the local temperature of the cells. Consequently, a first coupling between the CA and FE methods can be defined as a simple interpolation of the temperature of a cell ν , T_ν , from those calculated at the FE nodes n , T_n . Because the macro-time-step, Δt , used by the FE method does not necessarily fulfill the CA growth criterion (Eq. [2]), a micro-time-step, δt , is defined according to Eqs. [3] and [4]. The temperatures, T_ν^m , of a cell ν inside an element E_ν of the FE mesh at a given time $t_m \in [t, t + \Delta t]$ are thus deduced from linear interpolations on both time and space variables; *i.e.*,

$$T_\nu^m = \sum_{n \in E_\nu} \phi_n(\mathbf{x}_\nu) T_n^m \quad [5a]$$

$$T_n^m = T_n^t \frac{t + \Delta t - t_m}{\Delta t} + T_n^{t+\Delta t} \frac{t_m - t}{\Delta t} \quad [5b]$$

with $t_m \in [t, t + \Delta t]$

where the summation is performed on all the nodes belonging to the element E_ν and $\phi_n(\mathbf{x}_\nu)$ are the shape functions estimated at the cell center position, \mathbf{x}_ν . Similarly to the microenthalpy scheme defined in Reference 20, a loop on the micro-time-steps is therefore implemented and the CA nucleation and growth steps are repeated until $t_m = t + \sum \delta t = t + \Delta t$. The flow chart shown in Figure 2(a) summarizes the weak coupling scheme of the CAFE model.

The grain structure calculation can be performed interactively by calling the CA model within each macro-time-step of the FE method. But the main advantage of the weak coupling calculation mode is that the CA calculations can also be performed *a posteriori* once the FE calculation is completed, provided the FE mesh and temperature history have been stored on data files. This *postprocessing* method can be easily implemented into any finite element or finite difference codes.

B. Full Coupling Calculation Mode: Microenthalpy Scheme

In the weak coupling mode, the temperatures are calculated at the macro level using the FE mesh and a unique solidification path, *i.e.*, unique relationship between temperature and volume fraction of solid, f_s , or enthalpy, H . A more accurate coupling of the CA and FE methods consists of recalculating the temperature and fraction of solid of the FE nodes after each micro-time-step using the so-called “microenthalpy scheme,” first introduced by Thevoz *et al.*^[14,20] and already adapted for the 2-D CAFE model.^[1] Compared to a standard enthalpy method, such a scheme accounts for the delay in forming the solid due to the undercooling necessary for the formation of the dendritic structure. It thus leads to a better description of the latent heat release in the solidification interval, especially in a weak thermal gradient.

The FE code is based on an implicit enthalpy method to solve the heat flow equation during a macro-time-step. The procedure is as follows.

- (1) The enthalpy variations at the FE node locations, $\{\Delta H_n\}$, during one time-step are calculated using a linearization method^[20] and the known temperatures at time t , $\{T_n^t\}$.
- (2) The macro-time-step, Δt , is split into micro-time-steps, δt , and the variations of enthalpy at each node n of the FE mesh during one micro-time-step are linearized:

$$\delta H_n = \frac{\delta t}{\Delta t} \Delta H_n \quad [6]$$

i.e., the heat extraction rate is assumed to remain constant for each node during the macro-time-step, Δt .

- (3) For FE nodes whose temperatures are above the liquidus temperature or below the solidus temperature, the new temperatures, $\{T_n^{t+\Delta t}\}$, are simply deduced from the new enthalpies, $\{H_n^{t+\Delta t} = H_n^t + \Delta H_n\}$, using the $T(H)$ relationship used by the FE method.
- (4) For FE nodes located in the solidification interval, the following energy balance applies during one micro-time-step:

$$\delta H_n = \rho_p \delta T_n - L \delta f_{s,n} \quad [7]$$

where ρ_p and L are the volumetric heat capacity and latent heat of fusion, respectively. From Eqs. [6] and [7], it appears that the temperature variations at the FE node locations, δT_n , can be calculated if the variations of fraction of solid, $\delta f_{s,n}$, are known. Unlike the scheme introduced by Thevoz *et al.*,^[20] these later variations are calculated by summing the corresponding entities, $\delta f_{s,\nu}$, deduced for the cells (refer to subsequent explanations):

$$\delta f_{s,n} = \frac{\sum_{\nu} \phi_n(\mathbf{x}_\nu) \delta f_{s,\nu}}{\sum_{\nu} \phi_n(\mathbf{x}_\nu)} \quad [8]$$

The values of the new temperatures at each microtime, $\{T_n^{t+\delta t} = T_n^t + \delta T_n\}$, can thus be estimated using Eq. [7].

- (5) At the end of the macro-time-step, Δt , the new temperatures, $\{T_n^{t+\Delta t}\}$, and volume fractions of solid, $\{f_{s,n}^{t+\Delta t}\}$, at the FE node locations are known. The procedure is then restarted at point (1) for the following macro-time-step Δt .

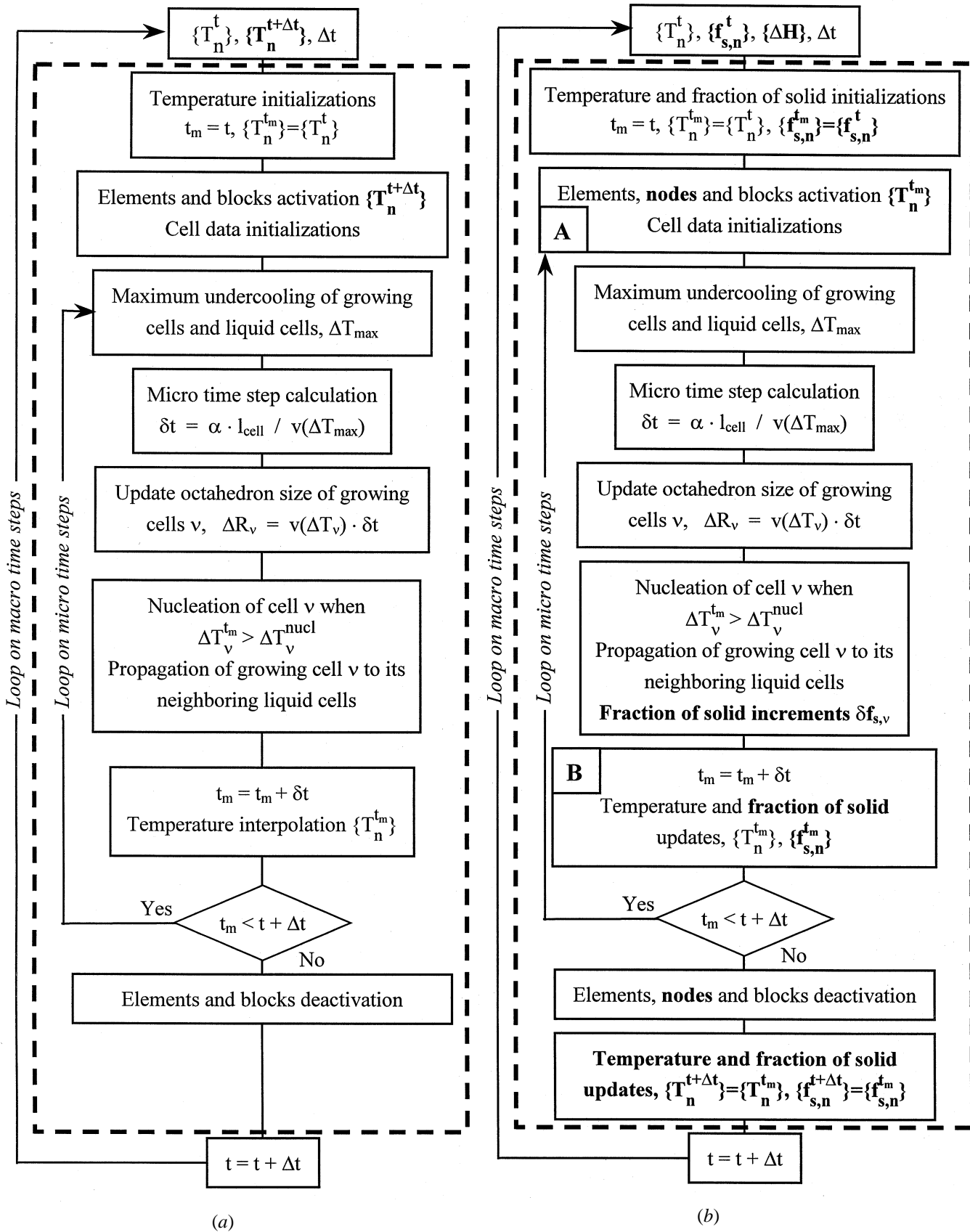


Fig. 2—Flow charts of the (a) weak and (b) full coupling calculation modes of the 3-D CAFE model.

The variation of the volume fraction of solid of a cell ν , $\delta f_{s,\nu}$, during one micro-time-step is computed following the coupling scheme proposed by Gandin and Rappaz.^[1] Three different situations are considered.

1. No variation of the fraction of solid

This situation is encountered for a cell completely solidified at the beginning of the micro-time-step (*i.e.*, with a temperature below the solidus temperature) or remaining liquid during the micro-time-step. In both cases, one has $\delta f_{s,\nu} = 0$.

2. Cell becoming mushy

Either due to nucleation or to the growth of an already mushy neighbor, the state index of a liquid cell changes to a nonzero value during the micro-time-step. The fraction of solid increment is then initialized using the Scheil microsegregation model^[13] at the actual temperature of the cell, T_ν^{tm} :

$$\delta f_{s,\nu} = 1 - \left(\frac{T_\nu^{tm} - T_m}{T_L - T_m} \right)^{1/(k-1)} \quad [9]$$

where T_L is the liquidus of the alloy, T_m is the melting point of the solvent, and k is the partition coefficient. This truncation of the Scheil relationship, which is identical to the assumption made in the model developed by Flood and Hunt,^[21] does not strictly conserve solute.^[22] It is nevertheless a fairly good approximation at the small undercoolings usually encountered in most solidification processes.

3. Solidification of a mushy cell

A mushy cell, *i.e.*, a cell with a nonzero state index and a nonzero fraction of solid, is solidified according to Scheil's microsegregation model. The derivative form of Scheil's equation (Eq. [9]) combined with a heat balance (Eq. [7]) written for a cell ν leads to

$$\delta f_{s,\nu} = \frac{-\delta H_\nu}{\rho c_p (T_L - T_m)(k-1)[1 - f_{s,\nu}^{tm(k-2)}] + L} \quad [10]$$

The enthalpy variation of cell ν , δH_ν , is deduced from a linear interpolation of the enthalpy variation of the FE nodes of the element to which the cell belongs. When the cell temperature reaches the eutectic temperature, T_E , an isothermal transformation is assumed to take place. The cell temperature is maintained at T_E as long as the fraction of solid is lower than unity and the increase of the solid fraction of the cell, $\delta f_{s,\nu}$, is calculated according to

$$\delta f_{s,\nu} = -\delta H_\nu / L \quad [11]$$

Figure 2(b) shows the flow chart of the full coupling calculation mode. Differences with the flow chart of Figure 2(a) valid for the weak coupling calculation mode have been highlighted in bold characters. In a sense, the integration of the microenthalpy scheme in the CAFE model can be viewed as a multigrid/multi-time-step technique.^[23] From interpolated enthalpy variations, variations of fraction of solid are calculated at the CA level and summed up at the FE node locations in order to deduce the new temperatures. It should be pointed out that the interpolation step with the shape functions, ϕ_n , is unique (Eq. [5a]), but the restriction from the CA level to the FE nodes (Eq. [8]) is not.^[23] The restriction step of the full coupling mode is labeled "B" in Figure 2(b). Also note that by decreasing the parameter α (Eq. [4]),

one can increase the number of micro-time-steps and, thus, avoid rebounding problems, as mentioned in Reference 20.

IV. DYNAMIC ALLOCATION

In order to predict successfully the competition occurring among columnar grains, Gandin and Rappaz have shown that the size of the CA cells should be smaller than the length at which the branching mechanisms of the dendritic network take place.^[1] As defined by Huang and Glicksman,^[24] this length is a function of the distance between "active" secondary dendrite arms, *i.e.*, branches extending into opened regions of liquid and leading to the formation of new tertiary arms. The tertiary dendrite arms may in turn transform into primary dendrite trunks in the case of directional solidification. In a particular case, a cell size $l_{\text{cell}} = 50 \mu\text{m}$ was found to be sufficient for a good prediction of the competition occurring among three columnar grains observed by Esaka in a succinonitrile-acetone alloy.^[1,25] In three dimensions, 10 million cubic cells of $50 \mu\text{m}$ would only correspond to a 1.25 cm^3 domain and yet require 1 GByte of RAM,* not counting the memory required for the

*About 100 bytes of information per cell is required in the CA algorithm

FE calculation. A 1.25 cm^3 volume is at least one order of magnitude too small to model a representative domain of a casting. Consequently, special dynamic allocation algorithms must be defined in order to model solidification grain structures in a representative volume of the casting, while avoiding definition of all the cells simultaneously. These are explained hereafter.

A. Window, Block, and Cell Subdivisions

In addition to the partitioning of the solidification domain into an FE mesh and a CA grid, two intermediate subdivisions are introduced: "blocks," which are sets of cells, and "windows," corresponding to sets of blocks (Figure 3).

Windows are orthogonal parallelepipeds whose faces are perpendicular to the (X, Y, Z) axes of the CA grid. Several windows, eventually contiguous, may be defined by the user and automatically numbered from 1 to N_w . The calculation domain for the microstructure is then defined as the intersection between these windows and the FE model of the cast part. Windows are used to limit the size of the calculation domain, and thus the number of cells, to zones of interest (*e.g.*, the grain selector or the region near a platform of a turbine blade).

Each window is made of blocks. A block is a set of $n_b = n_x \times n_y \times n_z$ cells, where n_x , n_y , and n_z are the numbers of cells in each block in the X, Y, and Z directions, respectively. All the blocks have the same size, *e.g.*, $n_x = n_y = 6$ in the case of Figure 3. For typically $n_x = n_y = n_z = 10$, the total number of blocks in the cellular automaton, N_B , is three orders of magnitude lower than the total number of cells. Blocks are indexed from 1 to N_B , starting in the first window and following the sequence of the N_w windows. In each window, the block index is incremented according to the CA axes (*i.e.*, X-axis first, Y-axis second, and Z-axis third). The total number of blocks in each window is also kept in memory. Therefore, given any block index between 1 and N_B , this absolute indexing scheme allows one to easily find

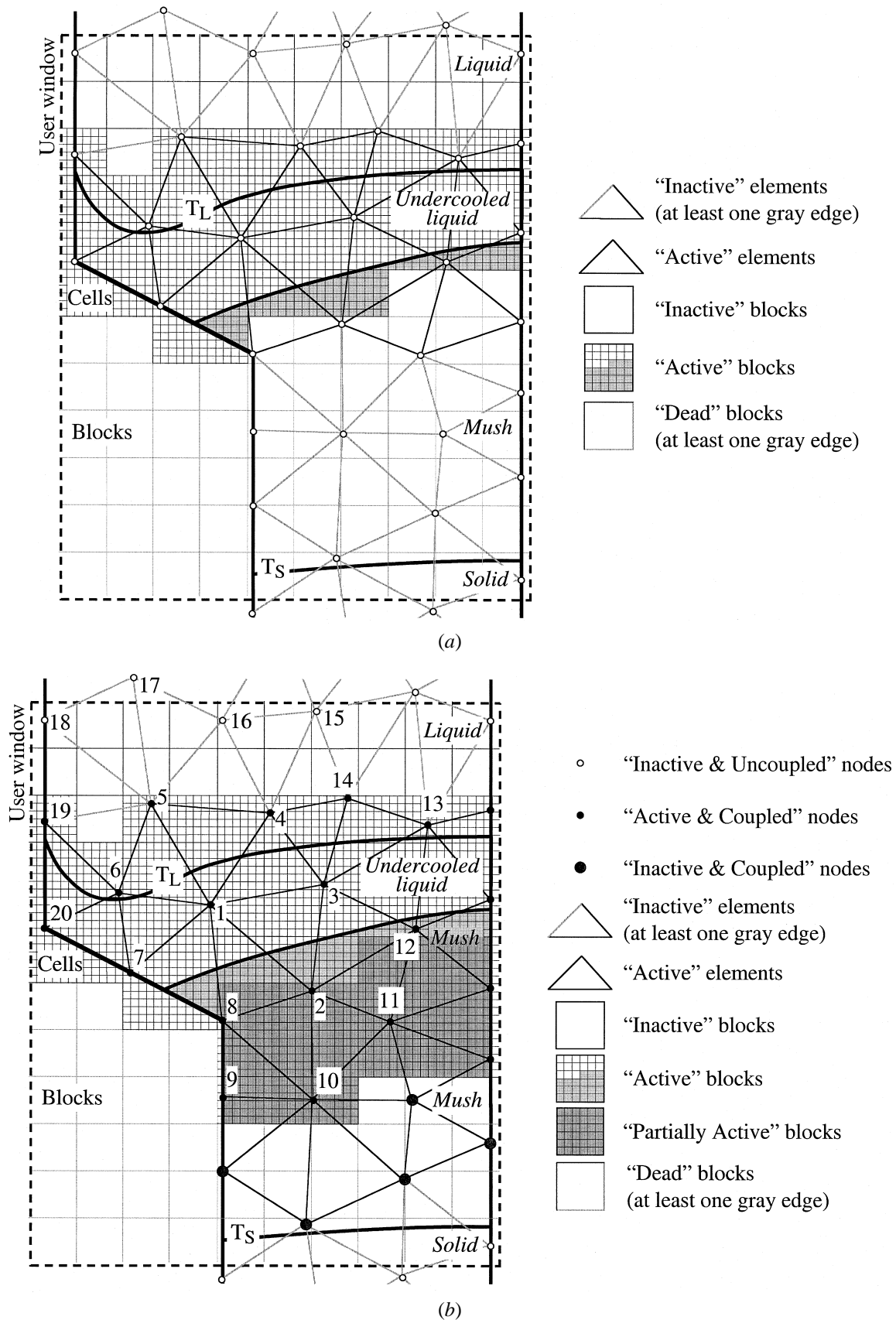


Fig. 3—Schematics of the dynamic allocation designed for the 3-D CAFE model in case of the (a) weak and (b) full coupling calculation modes. The window, block, and cell definitions are made visible in these figures. The state indexes of the nodes, elements, and blocks as a function of their position with respect to the current temperature field are also illustrated.

the window to which it belongs and its position in the window. In each block, the same numbering scheme is applied for the cells from 1 to n_b . Consequently, a cell is identified in a unique way in the entire cellular automaton grid by its block number (number in the range $[1, N_B]$) and its cell number in the block (number in the range $[1, n_b]$). It is to be noted that the blocks are subdivided into cells only when they become mushy, thus limiting drastically in most cases the memory size necessary for the CA calculations (as discussed subsequently).

B. Initializations (Finite Element-Block Connectivity Files)

In order to make interpolations-restrictions between FE nodes and CA cells (Eqs. [5a] and [8]), a certain number of interconnections must be defined also at the block level, prior to running a solidification calculation. A block belongs to a FE if at least one of its cells is inside the element. (Note that tests are performed considering the center of the cells with respect to the volume occupied by the FE). A list of all the blocks belonging to each element and another one defining all the elements to which a block belongs are constructed. These two connectivity tables are saved on two separate files called *finite element-block connectivity files*.

A state flag is attributed to each block. It is set to “dead” for blocks that do not belong to any element (*e.g.*, block falling entirely in the mold) and to “inactive” for the others. The state flag is the only element of information on the blocks permanently kept in the computer memory. For complex casting shapes that do not fit well in a single parallelepiped, the total number of dead blocks can be decreased by using contiguous windows whose union fits better the shape of the component (*e.g.*, two parallelepipeds for the bottom and upper platforms of a turbine blade and a thinner parallelepiped for the airfoil in between).

C. Activation and Deactivation of Blocks, Nodes and Elements, Cell References

During solidification, elements and blocks are activated, and then deactivated, in the CAFE calculation as the mushy zone moves across the domain. The procedures used to activate and deactivate elements and blocks, and thus to allocate and free the memory space associated with the CA cells, depend on the calculation mode specified by the user.

In the *weak coupling calculation mode*, elements are set active as soon as one of their nodes falls below the liquidus temperature. Because the temperature of the FE nodes is not modified by the CA module, the temperatures at the end of the macro-time-step, $\{T_n^{t+\Delta t}\}$, are used for the element and block activation. This procedure is thus carried out only once at each macro-time-step (Figure 2(a)). As illustrated in Figure 3(a), all the blocks that belong to the activated elements are themselves activated. This is done with the help of the FE-block connectivity file. All the variables needed for the CA model are then allocated into the memory. For instance, for each of the cells ν of a block being activated, the index of the finite element, E_ν , to which it belongs is calculated and stored. The search procedure for the determination of E_ν is restricted to the list of the elements to which the block belongs, as given by the corresponding

connectivity file. An arbitrary negative value for E_ν is assigned to each cell that does not belong to any element (*i.e.*, a cell falling in the mold but still belonging to a block that is not dead). Similarly, a reference index, I_{Ref} , is assigned to a cell that does not have all its first NN inside the calculation domain, *i.e.*, to a cell for which at least one NN cell has a negative E_ν value. The value I_{Ref} comes from the reference index of the corresponding FE boundary or from a reference index imposed on one face of a user window. Please note that optimizations are made so as to limit the total amount of variables. For instance, the coordinates of a cell, as well as the indexes of its first, second, and third NN are not stored in memory because they can be easily recalculated from the absolute indexing system used for the numbering of blocks and cells.

A block is deactivated when its n_b cells have ended their growth stage. Because the growth of a cell is considered until its 26 neighbor cells have turned mushy (or are dead), a block is deactivated when all its cells, as well as one layer of boundary cells belonging to the 26 adjacent blocks, are mushy. The memory space previously allocated to the cells of this block is then freed and the block is killed (flag index “dead” in Figure 3). Finally, if an active element contains only deactivated blocks, it is also deactivated (Figure 3).

In the *full coupling calculation mode*, the activation criterion of elements and blocks is essentially the same as for the weak coupling calculation mode. However, because the temperature variations during the macro-time-step are not known when entering the CA module, activation of elements, nodes, and blocks has to be updated at each micro-time-step using the explicit temperature, $\{T_n^m\}$, of the nodes (box labeled “A” in Figure 2(b)). In the 2-D CAFE model described in Reference 1, the increase of the fraction of solid of the FE nodes using Eqs. [8] through [11] was carried out until the temperature of the FE nodes fell below the eutectic temperature. This requires keeping in memory the data associated with the cells over the entire solidification interval of the alloy, $T_L - T_E$. A more efficient solution, which requires less memory, has been devised for the 3-D CAFE model.

For FE nodes located outside the CA windows, their new temperature and fraction of solid are directly computed from the enthalpy variations using a unique $T(H)$ relationship applied at the macroscale of the FE mesh. For FE nodes enclosed in the CA domain (*i.e.*, in the calculation windows defined by the user), two flags have been defined: an “Activation” flag (0 = Inactive, 1 = Active) and a “Coupling” flag (0 = Uncoupled, 1 = Coupled). These flags allow three different states of the FE nodes to be distinguished with respect to their coupling with the CA cells. This is illustrated in Figure 3(b). The state of a given FE node (*e.g.*, node 1 in Figure 3(b)) depends on the state of its *first- and second-NN environment*. The first-NN environment of an FE node n is made of all the nodes and associated elements directly connected to n (*e.g.*, volume outlined by nodes 2 through 8 in Figure 3(b) for node 1). The second-NN environment of a node n is made of all the nodes and associated elements directly connected to the nodes of the first-NN environment (*e.g.*, volume outlined by nodes 7 through 20 in Figure 3(b) for node 1).

(1) *Inactive and uncoupled FE nodes* (open circles in Figure 3(b)). This is the state of the FE nodes whose first-NN

environment is above the liquidus temperature. This is also the case of an FE node whose temperature is below T_E . The temperature of such nodes at time t_m is simply updated using Eqs. [6] and [7] with a zero increment of the fraction of solid, $\delta f_{s,n} = 0$.

- (2) *Active and coupled FE nodes* (filled circles in Figure 3(b)). An FE node is set “Active” and “Coupled” when at least one liquid cell of its first-NN environment is undercooled. It remains “Active” and “Coupled” when at least one liquid cell of its second-NN environment is undercooled. The fraction of solid and temperature of such a node is updated using the microenthalpy scheme coupled with the CA model (Eqs. [6] through [11]).
- (3) *Inactive and coupled FE nodes* (gray filled circles in Figure 3(b)). For an FE node not defined by (1) or (2), the increment of the fraction of solid, $\delta f_{s,n}$, is directly computed from its microenthalpy variation, δH_n , using Eq. [10] written for node n . This means that the update of the fraction of solid and temperature of such FE nodes is no longer calculated using the CA model. When the temperature of these nodes reaches the eutectic temperature, an isothermal transformation is performed until their fraction of solid, $f_{s,n}$, reaches unity (Eq. [11] written for node n is directly applied to δH_n). The flags of the nodes are switched to the “Inactive” and “Uncoupled” states once the fraction of solid reaches unity (case (1)).

For the activation of the blocks, the same criterion defined in the weak coupling calculation mode is applied. However, the deactivation of the blocks is made in two steps in order to optimize the memory allocation. A first partial release of the memory is made when all the cells of a block and the NN cells of adjacent blocks are no longer liquid (similar to the deactivation procedure used in the weak coupling case). This memory release is accompanied by a block flag index switch from “Active” to “Partially Active.” In the partially active block state, some variables are still kept in memory (e.g., the fraction of solid of the cells is still used to compute the fraction of solid update of the nodes through stage (2)), whereas others are no longer used (e.g., octahedron size associated with the cells). A block is switched from “Partially Active” to “Dead” (and the associated memory is totally released) when all its connected finite elements have all their nodes in a first-NN environment which does not contain any liquid cell.

V. APPLICATIONS

A. Automatic Generation of CA Grid

As mentioned in Section IV, one of the main difficulties associated with the implementation of the 3-D CAFE model is the dynamic allocation of the cells. A preliminary difficulty is the definition of the blocks and cells, with proper assignment of reference indexes to cells belonging to external and internal boundaries, from the FE mesh. This has to be done automatically without additional work, and specific routines have been developed for that purpose.

Figure 4 illustrates the automatic creation of the (b) CA grid from the (a) FE mesh of a turbine blade geometry. Only a close-up detail of the junction between the “pigtail” selector and the blade platform is shown. The typical cell size used in the CA calculation is 50 to 100 μm .

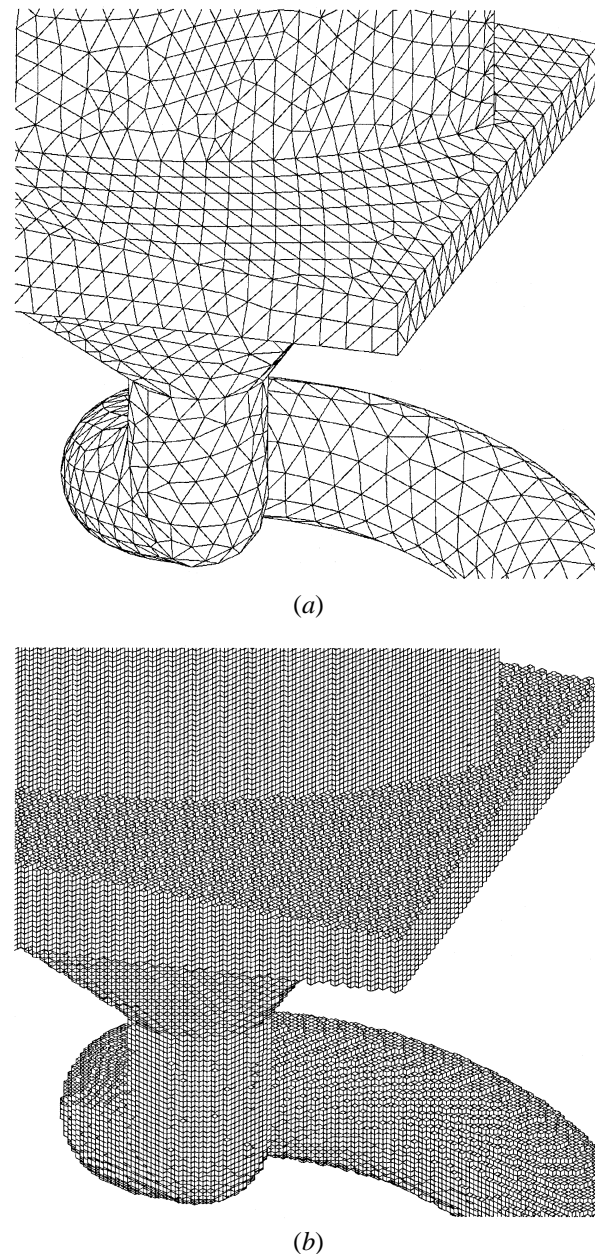


Fig. 4—Automatic generation of (b) a cubic cell lattice used by the CA model from (a) the FE mesh in the platform of a single-crystal turbine blade geometry located at the exit of a pigtail grain selector.

B. Directionally Solidified Turbine Blade

Figure 5 presents the grain structure of a DS turbine blade cast by the Snecma (Paris, France) airplane engine company as calculated with the 3-D CAFE model in the weak coupling mode. The casting is made of a nearly parallelepipedic starter block, which was in contact with a copper chill, above which stands the blade itself. The computation data used in the simulation (cell size, number of cells, number of elements, and micro-time-step parameter) are given in Table II. The enmeshment, as well as the temperature files, have been calculated by Snecma using the software ProCAST. Because the number of cells in the blade is fairly large, specific storage and graphic tools have also been designed in order to minimize the result file size and the display time. In the example shown here, only the “skin” cells of the casting

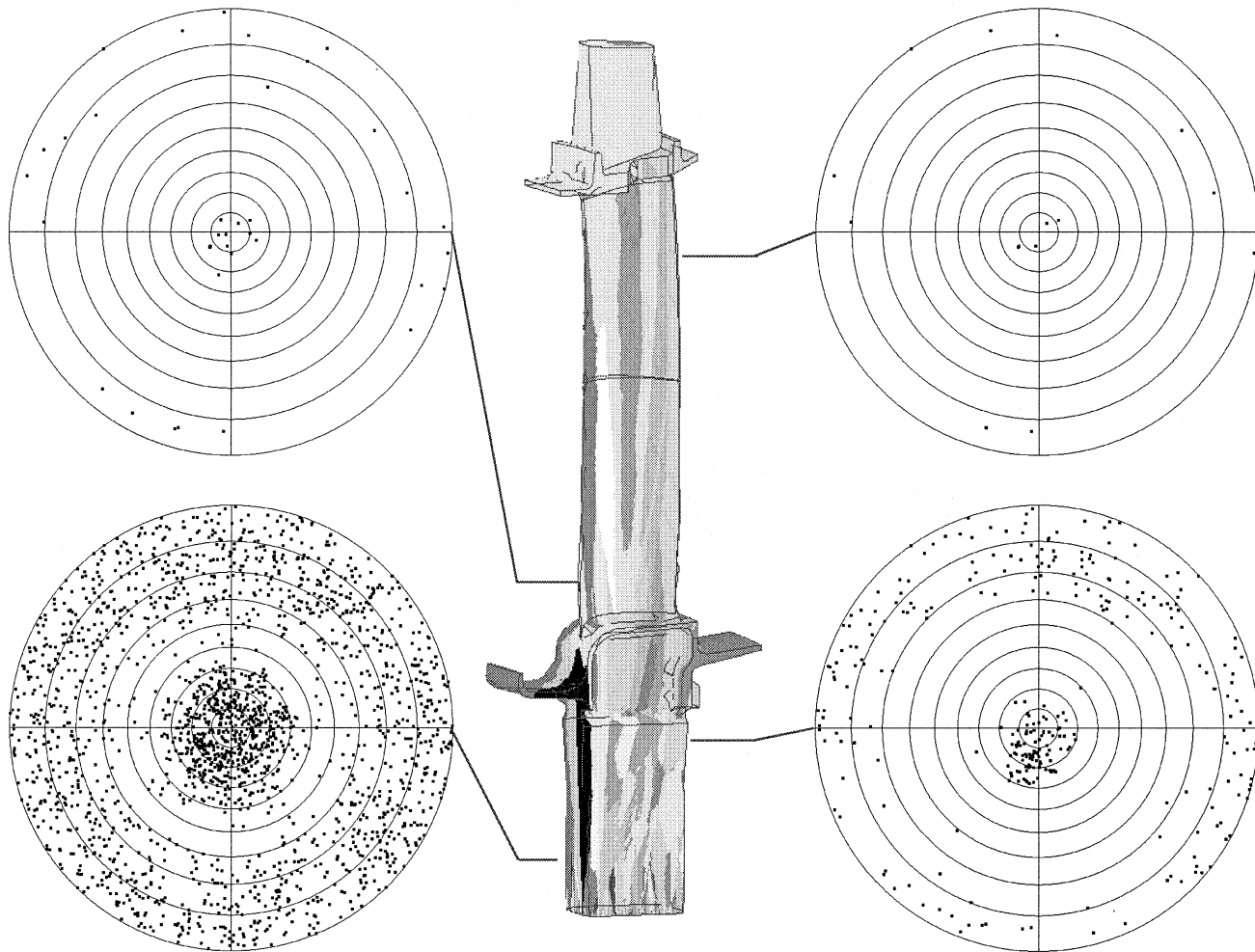


Fig. 5—A 3-D view of the final grain structure calculated in the weak coupling mode for a DS turbine blade. The $\langle 100 \rangle$ pole figures are displayed for various cross-sections perpendicular to the main blade axis (geometry provided by Snecma, Paris, France; calculation parameters listed in Table II).

Table II. Calculation Parameters and CPU Time (SGI R4400 at 250 MHz)

	Directionally Cast Blade (Figure 5)	Pigtail Grain Selector (Figure 6)	Continuously Cast Rod (<i>a/b</i>) (Figure 7)
Cell size, l_{cell} (μm)	100	100	50
Micro-time-step parameter, α	1.0	0.5	0.2
Number of FE nodes in casting	34,851	9,655	23,040
Number of cells	21,682,938	2,698,391	18,732,000
CPU time*	5 h 35 min	1 h 17 min	16 h 37 min/26 h 31 min

*For the continuously cast rods, the CPU time also includes the heat flow computation. The CPU times cannot be directly compared because the simulated times and their divisions in macro-time-steps are not the same.

have been displayed: these are the cells that have a nonzero boundary reference index. Other graphical features implemented in the CAFE postprocessing are the visualization of grain structures in selected cross-sections parallel to the main axes of the CA grid, growth front at selected times (cells having at least one liquid neighbor cell at the corresponding times), nucleation centers, undercooling of the cells at their time of capture, *etc.*

The grains in Figure 5 are colored with different gray

levels. As can be seen, the DS blade is made of long columnar grains nucleated at the bottom part of the casting. As noted in previous work,^[6] the transverse size of these grains is increasing with the distance from the nucleation surface (bottom part of the casting in contact with a chill surface). This is due to the growth competition of dendrites at grain boundaries, which is also responsible for the evolution of the crystallographic orientation of the grains. From a random orientation at the nucleation surface, the grains that remain

during the selection process are those that have one of their $\langle 100 \rangle$ directions most closely aligned with the thermal gradient. In the DS blade of Figure 5, this direction nearly corresponds to its longitudinal axis. The preferential $\langle 100 \rangle$ growth directions of dendritic grains being accounted for in the 3-D CA growth algorithm, the evolution of the texture is part of the prediction of the CAFE model. This evolution is illustrated in Figure 5 for the same blade: the $\langle 100 \rangle$ pole figures of the grains seen in four cross-sections taken at various heights of the casting are displayed. The centers of these pole figures correspond to the main axis of the blade. As can be seen, grain selection has already occurred at the level of the lowest pole figure, only a few millimeters above the nucleation surface. At the exit of the starter block (second pole figure), the remaining grains have their $\langle 100 \rangle$ trunk direction within a cone of semiapex smaller than 20 deg. Please note that the cloud of points corresponding to these directions is not precisely centered in the pole figure, the thermal gradient being slightly misoriented with respect to the blade axis. The role of the starter block is clearly evidenced by the 3-D CAFE simulation: the grains starting to grow in the blade itself have their $\langle 100 \rangle$ directions well aligned with the blade axis. Nevertheless, grain selection continues to operate in the blade and only five grains remain in the upper part.

The number of grains in a DS airfoil is a common inspection criterion used in quality assurance. As can be seen, the 3-D CAFE model provides such information. It also predicts the grain structure evolution near a platform, which is an important issue, especially for the larger blades used in land-base gas turbines. The CPU time listed in Table II corresponds in this case only to the CA calculation, using a previously calculated temperature field. It is in this case smaller than the time required for the FE calculation of heat diffusion and radiation. However, it should be pointed out that the fairly coarse CA grid used here (100 μm) slightly biases the prediction of grain selection; the result shown here is therefore only qualitative. More accurate results could be obtained by using a finer grid, but the CPU time, file size, and display time would increase accordingly. For that reason, the possibility of "windowing" selected areas has been implemented in the 3-D CAFE model.

The selection mechanism and texture formation of columnar grains illustrated in Figure 5 have already been investigated, both experimentally and numerically, by Gandin *et al.*^[6] This analysis was performed using a simplified CA algorithm valid for a uniform temperature field. Refined investigations using the present 3-D CAFE model have been reported in Reference 26.

C. Single Grain Selection for Investment Cast Parts

The production of single-crystal turbine blades precisely uses the grain selection mechanism described earlier in a complex starter geometry, which eliminates all the grains but one. The most frequently used geometry is a "pigtail" selector such as the one shown in Figure 6 (a), and also partially shown in Figure 4. Until now, the design of such a grain selector was entirely based on trial and error, whereas the 3-D CAFE model provides a new and unique tool for its study and optimization.

Figure 6(a) shows the grain structure in the pigtail selector

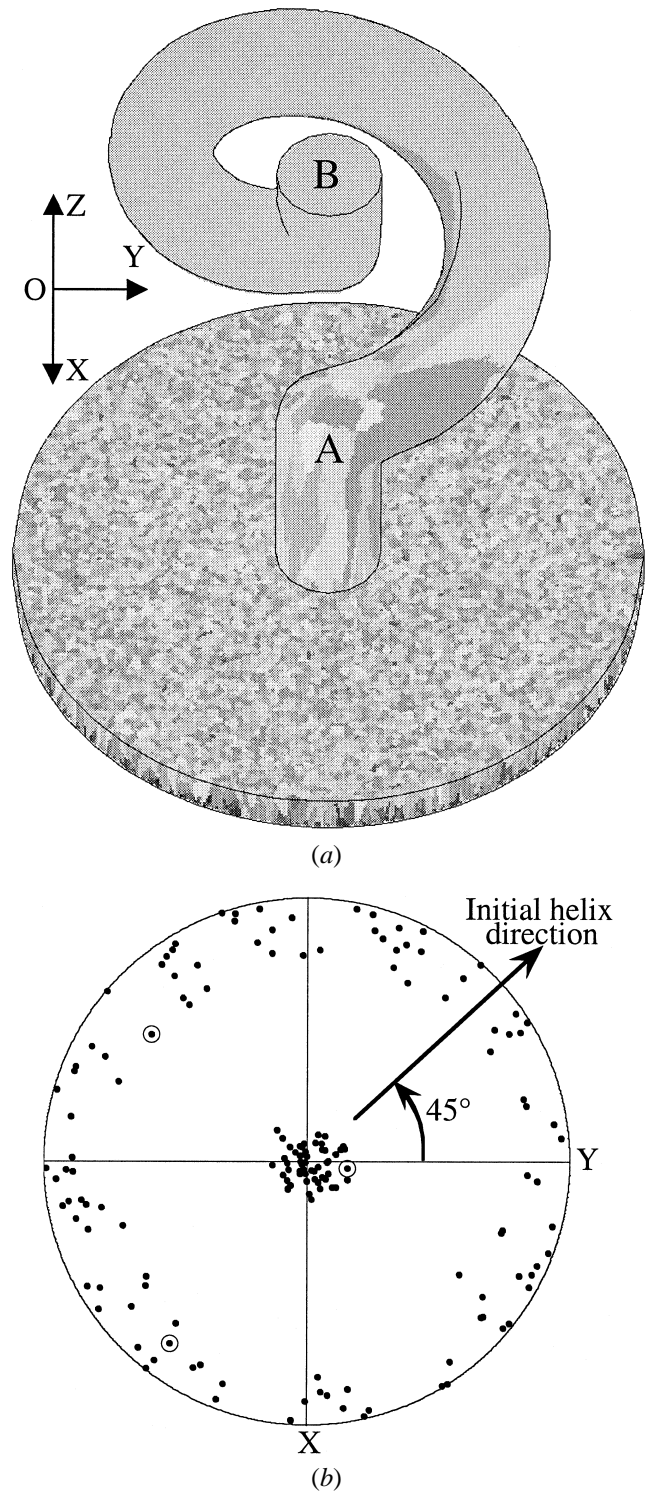


Fig. 6—(a) A 3-D computed columnar structure in a pigtail grain selector used for the production of single-crystal turbine blades by investment casting and (b) a pole figure of the $\langle 100 \rangle$ crystallographic directions at the level of section A. The center of the projection corresponds to the Z direction, *i.e.*, the normal to the bottom surface in contact with the chill. The three circled dots in the pole figure correspond to the $\langle 100 \rangle$ directions of the selected grain seen in the upper section B (calculation parameters listed in Table II).

as predicted with the 3-D CAFE model. This pigtail selector connects a thin disk in contact with a copper chill and the

bottom platform of the blade (Figure 4). A very high flux is applied at the disk-chill interface, whereas the other surfaces of the casting can be considered as nearly adiabatic. Indeed, the ceramic mold and insulation materials have very low thermal conductivities as compared with that of the metal. Accordingly, the thermal gradient direction follows the axis of the bottom disk and of the helix selector. In this simulation, the nucleation parameters are only defined for the disk-chill boundary. A sharp Gaussian distribution has been chosen, simulating a burst of nucleation just below the liquidus temperature. As can be seen, many grains form in the bottom section of the pigtail. Some of them enter the restriction of the vertical section of the pigtail selector. At the level of section A, about 50 grains have survived to the grain competition, as can be seen in the associated $\langle 100 \rangle$ pole figure shown in Figure 6 (b). These grains have their $\langle 100 \rangle$ dendrite trunk direction close to the Z-axis, which is perpendicular to the chill surface. At the level of section A, this direction is also that of the thermal gradient.

As the grains enter now in the helix part of the pigtail, they see a thermal gradient direction that continuously evolves along the spiral line. The grain competition in this complex thermal environment leads to the selection of only one grain at the exit of the selector (section B). This grain, whose $\langle 100 \rangle$ crystallographic directions are identified by small circles in Figure 6(b), can then extend freely in the whole part to form a single-crystal turbine blade. Please note that the projection onto a XY plane of the helix direction starting just above section A is given by the arrow drawn in Figure 6(b). It corresponds to a rotation of about 45 deg with respect to the Y-axis. As can be seen, one of the $\langle 100 \rangle$ crystallographic directions of the selected grain remaining in section B is nearly aligned with this initial helix direction (in fact, this direction points slightly toward the Z direction and thus appears in the opposite quadrant of the pole figure.) Thus, the pigtail has selected one of the grains having a secondary dendrite arm closely aligned with its initial helix direction. As clearly emphasized by the CAFE calculation, the selection of the secondary dendrite arms could be used to produce a turbine blade whose primary and secondary $\langle 100 \rangle$ dendrite arm directions are oriented with respect to the in-service mechanical stress state.

D. Continuously Cast Rods

The final example shown in this article concerns the continuous casting of small rods. The 2-D CAFE model was already applied to such a process;^[3] the extension to 3-D of these predictions is displayed in Figure 7. In this case, the FE heat flow simulation was performed for a long cylinder (about 3 times as long as that shown in Figure 7). Once a stationary temperature profile was reached, the CA calculation was started from a fictitious bottom surface on which nucleation could occur. After some distance, a "stationary" grain structure is obtained. It is shown in Figure 7 for two different casting speeds: the transverse sections correspond to a steady state, whereas the longitudinal sections allow viewing of the grains from the bottom nucleation surface up to the solid-liquid interface. (a) at low speed, the liquidus isotherm is fairly flat, whereas (b) at higher speed, the sump is much deeper. In the first case, the grains are nearly parallel to the rod axis and appear as "equiaxed" in the transverse section. In the second case, they grow inward from the

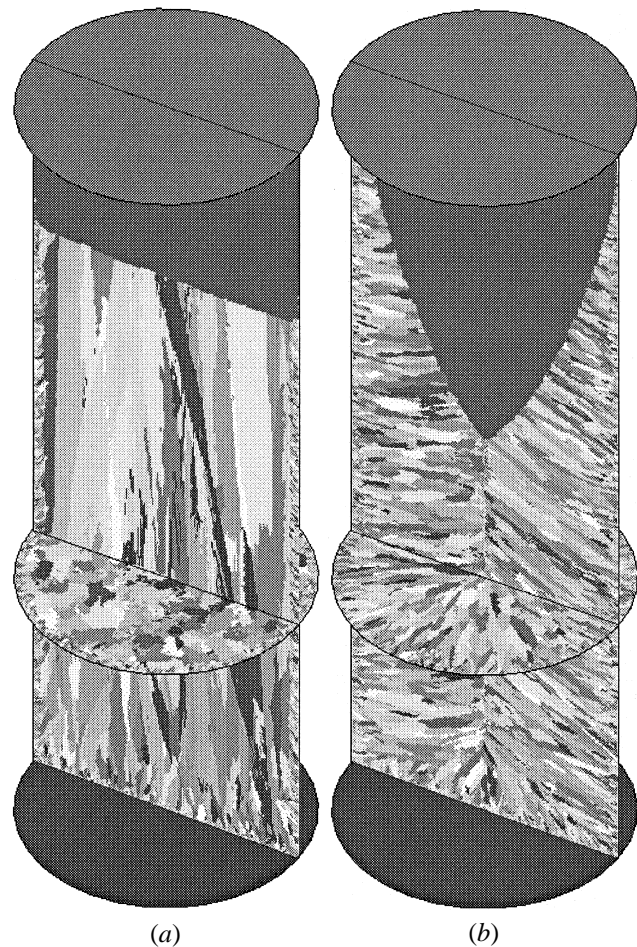


Fig. 7—Predicted 3-D grain structures in aluminum-silicon rods that have been continuously cast at (a) low and (b) high speeds. The grains are shown in longitudinal and transverse sections (calculation parameters listed in Table II).

surface and thus appear rather columnar in both longitudinal and transverse sections. Please note that at low speed, a small cortical zone of grains nucleated at the lateral surface of the rods is also present. The growth of these grains is not favored in the nearly vertical temperature gradient and the long columnar grains issued from the nucleation bottom surface stop them. Although a high solidification rate is preferred for economical reasons, the grain structure of Figure 7(b) is often undesirable. Indeed, the grains grow perpendicularly to the surface of the rods, and they meet at the centerline, thus possibly creating a centerline segregation detrimental to the extrusion or rolling properties.

VI. CONCLUSIONS

The 3-D CAFE model presented in this article is shown to reproduce features of solidification grain structures that were never previously modeled. In particular, the growth competition occurring among columnar grains is directly reproduced, taking into account the crystallographic orientation of the grains and the temperature evolution in representative 3-D parts. The CAFE model also predicts the growth of equiaxed grain structures. In fact, the main advantage of the CA technique coupled with an FE method is that the grains are either columnar or equiaxed as a direct result of

the local solidification conditions (*i.e.*, thermal gradient and cooling rate). It is thus a unique technique for the modeling of grain structure transitions; both the columnar-to-equiaxed and equiaxed-to-columnar transitions, previously modeled using the 2-D CAFE model,^[1,27] can be reproduced using the 3-D CAFE model.

Industrial interest of investment casting companies has clearly been expressed through the funding of the project, which led to the results presented in this article. It was justified by the fact that they wanted to improve their solidification process by a better understanding and control of the grain structures formed during casting, including texture formation in the as-cast products. As demonstrated, the 3-D CAFE model can be used to design and optimize grain selectors used for the production of single-crystal turbine blades. The major advantage is then a direct visualization of the effect of the thermal history on the formation of the 3-D grain structure, while deducing from the calculation the evolution of both the grain density and texture. Several stochastic calculations could also be done in order to deduce the statistical efficiency of a given selector geometry and its cooling conditions.^[28]

It is believed that the 3-D CAFE model can find other fields of application because the physical mechanisms of nucleation and growth of dendritic grains, which are embedded into the CA algorithms, are clearly common to several solidification processes. The formation of the grain structure in continuously cast rods could be one of the processes to benefit from such developments. It would also be interesting to see if, in the future, the 3-D CAFE model could be coupled with other fields of materials science and engineering. As a matter of fact, 3-D simulated grain structures can be used as the input for the prediction of some mechanical properties of as-cast components or of defects associated with grain boundary (*e.g.*, hot tearing).

ACKNOWLEDGMENTS

This project has been funded by the Commission pour la Technologie et l'Innovation (Bern, Switzerland) (Grant No. 2861.1) and by a consortium of companies: ABB Management Ltd. (Baden, Switzerland), Calcom S.A. (Lausanne, Switzerland), Howmet Corporation (Whitehall, MI), PCC Airfoils Inc. (Beachwood, OH), Rolls Royce Plc (Derby, United Kingdom), Snecma (Paris, France), and T&N Technology/AE Turbine Component Ltd. (Leeds, United Kingdom). The authors thank Jean-François Joyeux and Marek Swierkosz (Calcom S.A., Switzerland) for the development

of the pre- and postprocessing modules of the 3-D CAFE software.

REFERENCES

1. Ch.-A. Gandin and M. Rappaz: *Acta Metall. Mater.*, 1994, vol. 42, pp. 2233-46.
2. Ch.-A. Gandin, R.J. Schaefer, and M. Rappaz: *Acta Mater.*, 1996, vol. 44, pp. 3339-47.
3. M. Rappaz, Ch.-A. Gandin, J.-L. Desbiolles, and Ph. Thevoz: *Metall. Mater. Trans. A*, 1996, vol. 27A, pp. 695-705.
4. Ch.-A. Gandin, M. Rappaz, and R. Tintillier: *Metall. Trans. A*, 1993, vol. 24A, pp. 467-79.
5. Ch.-A. Gandin, M. Rappaz, and R. Tintillier: *Metall. Mater. Trans. A*, 1994, vol. 25A, pp. 629-35.
6. Ch.-A. Gandin, M. Rappaz, D. West, and B.L. Adams: *Metall. Mater. Trans. A*, 1995, vol. 26A, pp. 1543-52.
7. Ch.-A. Gandin and M. Rappaz: *Acta Metall. Mater.*, 1997, vol. 45, pp. 2187-95.
8. T. Toffoli and N. Margolus: *Cellular Automata Machines*, The MIT Press, Cambridge, MA, 1987.
9. S.G.R. Brown and J.A. Spittle: *Mater. Sci. Technol.*, 1989, vol. 5, pp. 362-68.
10. J.A. Spittle and S.G.R. Brown: *Acta Metall.*, 1989, vol. 37, pp. 1803-10.
11. P. Zhu and W. Smith: *Acta Metall.*, 1992, vol. 40, pp. 683-92.
12. P. Zhu and W. Smith: *Acta Metall.*, 1992, vol. 40, pp. 3369-79.
13. W. Kurz and D.J. Fisher: *Fundamentals of Solidification*, Trans Tech Publications, Aedermannsdorf, Switzerland, 1989.
14. M. Rappaz: *Int. Mater. Rev.*, 1989, vol. 34, pp. 93-123.
15. D. Turnbull: *J. Chem. Phys.*, 1949, vol. 18, pp. 198-203.
16. H.J. Bunge: *Texture Analysis in Materials Science*, Butterworth and Co., London, 1982.
17. W. Kurz, B. Giovanola, and R. Trivedi: *Acta Metall.*, 1986, vol. 34, pp. 823-30.
18. M. Bobadilla, J. Lacaze, and G. Lesoult: *J. Cryst. Growth*, 1988, vol. 89, pp. 531-44.
19. D.E. Ovsienko, G.A. Alfintsey, and V.V. Maslov: *J. Cryst. Growth*, 1974, vol. 26, pp. 233-38.
20. Ph. Thevoz, J.-L. Desbiolles, and M. Rappaz: *Metall. Trans. A*, 1989, vol. 20A, pp. 311-22.
21. S.-C. Flood and J.D. Hunt: *J. Cryst. Growth*, 1987, vol. 82, pp. 543-51 and 552-60.
22. W.J. Boettinger, U.R. Kattner, and D.K. Banerjee: in *Modeling of Casting, Welding and Advanced Solidification Processes VIII*, B.G. Thomas and C. Beckermann, eds., TMS, Warrendale, PA, 1998, pp. 159-70.
23. A. Brandt: *Math. Comput.*, 1997, vol. 31, pp. 333-90.
24. S.C. Huang and M.E. Glicksman: *Acta Metall.*, 1981, vol. 29, pp. 701-15 and 717-34.
25. H. Esaka: Ph.D. Thesis, Ecole Polytechnique Federale de Lausanne, Lausanne, 1986, no. 615.
26. 3-D Stochastic Modelling of Microstructures, Final Report (1998), Ecole Polytechnique Federale de Lausanne, Lausanne, Switzerland, and Calcom S.A., Lausanne, Switzerland.
27. Ch.-A. Gandin, t. Jalanti, and M. Rappaz: in *Modeling of Casting, Welding and Advanced Solidification Processes VIII*, B.G. Thomas and C. Beckermann eds., TMS, Warrendale, PA, 1998, pp. 363-74.
28. Ch.-A. Gandin, M. Rappaz, J.-L. Desbiolles, E. Lopez, M. Swierkosz, and P. Thevoz: in *Superalloys 718, 625, 706 and Various Derivatives*, E.A. Loria, eds., TMS, Warrendale, PA, 1997, pp. 121-30.